Columnar Optical Depth and Vertical Distribution of Aerosols over Shanghai

Xuan Jia[1], Tiantao Cheng[1*], Jianmin Chen[1], Junwei Xu[1], Yonghang Chen[2]**

[1] *Department of Environmental Science and Engineering, Fudan University, Shanghai 200433, China*
[2] *College of Environmental Science and Engineering, Donghua University, Shanghai 201620, China*

ABSTRACT

The vertical distributions and optical properties of aerosols over Shanghai were analyzed using data from ground-based observation, space remote sensing and trajectories. Measurements of spectral aerosol optical depth (AOD) were carried out at Shanghai using a hand-held multi-band sun photometer MICROTOPS II from November 2009 to October 2010. AODs were almost in low level during the entire experiment, especially in the period of the World Exhibition/Exposition (EXPO) 2010. And, the daily-averaged AODs showed a clear pattern of seasonal variation, with maximum 0.69 in November and minimum 0.24 in August. Angstrom exponents were commonly exceeding 1.30, indicating that fine particles mainly contributed to aerosol loading except springtime. Based on Cloud-Aerosol Lidar and Infrared Pathfinder Satellite Observation/Cloud-Aerosol Lidar with Orthogonal Polarization (CALIPSO/CALIOP) retrieval and air back-trajectory modeling, the vertical distribution of aerosols were examined and classified into near-surface, mixed and multilayer transport types. The results denote the effects of aerosols from local sources or/and transported from remote sources on aerosol loadings. Comparison of AODs derived from CALIOP with those from ground observation revealed a reliable agreement with a correlative coefficient of 0.59. The variety of the aerosol types of Shanghai probably is the main contributor of the uncertainties.

Keywords: Aerosol optical depth; Vertical extinction profile; CALPSO/CALIOP.

INTRODUCTION

Aerosols play an important role in the global climate system through modifications of the global radiation budget. However, the radiative forcing of aerosols remains dominant uncertainty in understanding climate change due to their short lifetime, various chemical and physical characteristics and complex spatio-temporal distribution (IPCC, 2007). Particularly, information about tropospheric aerosol vertical distributions and optical properties is of paramount importance and necessary for precise radiative transfer calculation (Kaufman *et al.*, 1997; Yu *et al.*, 2006).

Over the past decades, a number of studies on aerosol vertical distributions have been done by ground observation, remote sensing and modeling, including observation of some special pollution events such as dust storm and forest-fire smoke, analysis of vertical distributions of aerosol optical properties under different conditions and their effects on solar heating, and estimation of ground-level particulate matter concentrations from AOD, etc. (Murayama *et al.*, 2004; Donkelaar *et al.*, 2006; Chiang *et al.*, 2007; He *et al.*, 2008; Huang *et al.*, 2008a, b; Chen *et al.*, 2009; Wang *et al.*, 2010). The NASA Micro-Pulse Lidar Network (MPLNET) provides standardized and coordinated measurements of aerosol vertical distributions using a federated network of Micro-Pulse Lidar system, which has several sites collocated with the NASA Aerosol Robotic Network (AERONET) (Welton *et al.*, 2001). The Cloud-Aerosol Lidar and Infrared Pathfinder Satellite Observation/ Cloud-Aerosol Lidar with Orthogonal Polarization (CALIPSO/CALIOP) has acquired global aerosol vertical profiles since June 2006 (Winker *et al.*, 2010). These projects give a chance to understand aerosol vertical distributions on a global scale (Royer *et al.*, 2010; Yu *et al.*, 2010). In eastern Asia, several international field campaigns such as ACE-Asia and ABC projects and regional scale studies in major cities have been conducted in recent years (Shimizu *et al.*, 2004; Nakajima *et al.*, 2007; Zhang *et al.*, 2009; Hara *et al.*, 2011; Hatakeyama *et al.*, 2011). These studies provide useful information of aerosol micro-physical, chemical, and radiative properties.

As one of the most developed cities of China, Shanghai suffers heavy aerosol loadings caused by local pollution and transport of remote source emissions. Furthermore, air

* Corresponding author. Tel.: +86-21-65642521;
  Fax: +86-21-65642080
  E-mail address: ttcheng@fudan.edu.cn (Tiantao Cheng)
** Corresponding author. Tel.: +86-21-65642298;
  Fax: +86-21-65642080
  E-mail address: jmchen@fudan.edu.cn (Jianmin Chen)

masses from the East China Sea and the Hangzhou Bay bring sea-salt aerosols and water vapor to complicate aerosol optical properties in Shanghai, especially in summertime. Studies on aerosol properties over the Yangtze River Delta (YRD) including Shanghai indicated that aerosol loading was increasing dramatically for recent decades over this region (Luo *et al.*, 2002; Duan *et al.*, 2007; Xiao *et al.*, 2011). Pan *et al.* (2010) analyzed and compared the aerosol optical properties of five sites located within the YRD region. He *et al.* (2010) compared MODIS derived AODs with sun photometer measurements of seven sites in the YRD region and suggested that the complicated aerosols properties and underlying surface types would probably be the reasons of retrieval errors. However, few studies have taken aerosol vertical distribution into consideration, although it would benefit to further understanding of air pollution and improving radiative forcing calculation.

This study aimed to analyze the vertical distributions and optical properties of aerosols over Shanghai. Variation of AODs and Angstrom exponent, and the aerosol extinction profiles from November 2009 to October 2010 were studied. The results of ground-based observation, space remote sensing and trajectory analysis would provide insights into the relationship among aerosol optical properties, its vertical distribution, and aerosol transport mechanism in the atmosphere.

MEASUREMENTS AND METHODOLOGY

Site Description

AOD measurements in this study were performed on the roof of No.4 teaching building (31.3°N, 121.5°E) about 20 m height above the ground in the campus of Fudan University in Shanghai. This site is representative of urban district due to the influence of residential, traffic, and construction emissions.

Sun Photometer

A hand-held multi-band sun photometer MICROTOPS II (Solar Light Company, USA) was used to measure AODs at five wavelengths of 340, 500, 675, 870 and 1020 nm. The accuracy of wavelength channels is ± 0.3 nm in UV range and ± 1.5 nm in visible and near-infrared ranges. Optical depth of O_3 absorption is ignored in MICROTOPS II. More details about the performance and data acquisition methodology of the instrument are reported in the literatures (Morys *et al.*, 2001; Ichoku *et al.*, 2002). The instrument was calibrated using comparison Microtops with a more accurate instrument before experiments, and using the standard Langley plots technique on cloud-free days in every month during the entire campaign (Ichoku *et al.*, 2002). The front quartz window of the instrument was clean regularly for keeping accuracy of data. During the campaign, a tripod was used to keep stable during observation and minimize the sun targeting error. First of all, to avoid cloud contamination, Microtops measurements were conducted on days that are as cloud-free as possible, and in any case, when there is no cloud patch covering or even close to the line of sight to the Sun. When possible, measurements were conducted around the local solar transit time (local solar noon) in order to limit the effect of optical distortions due to large solar zenith angles. Totally, one-year AODs were collected in the time of 11:00–16:00 LT (local time) at a 45–60 minutes interval from November 2009 to October 2010. And, 2 or 3 parallel measurements were made each time when AODs were collected to assure the quality of data.

CALIPSO/CALIOP

The Cloud-Aerosol Lidar with Orthogonal Polarization (CALIOP) is a near-nadir viewing two-wavelength polarization-sensitive lidar carried by CALIPSO satellite. Its 705 km-height sun-synchronous orbit has a repetitivity of 16 days. The laser built around Nd:YAG can produce simultaneous coaligned pulses at 1064 nm and 532 nm with a mean pulse energy of 110 mJ and a repetition rate of 20.25 Hz (i.e. a horizontal resolution of 333 m). The backscatter signals at 1064 nm and the parallel and perpendicular components of 532 nm are collected by a 1-m diameter telescope. Unlike the current generation of space-based remote sensing instruments, CALIOP provides high vertical resolution (30 m for –0.5–8.2 km and 60 m for 8.2–20.2 km) and allows retrieval of aerosol profile at night, over bright surfaces and above lower-lying cloud or beneath optical thin clouds as well as in clear sky conditions (Hunt *et al.*, 2009; Winker *et al.*, 2010).

The Level 2 CALIOP aerosol product retrieval scheme is composed of a feature detection scheme, a module that classifies features according to layer type (e.g., cloud vs. aerosol) and sub-type, and finally an extinction retrieval algorithm that estimates aerosol backscatter, extinction coefficient profile and total column aerosol optical depth (AOD) using an "assumed" extinction-to-backscatter ratio (LR) for each detected aerosol layer (Winker *et al.*, 2009). There are 6 different aerosol types: polluted continental (LR = 70 sr at 532 nm), biomass burning (LR = 70 sr at 532 nm), desert dust (LR = 40 sr at 532 nm), polluted dust (LR = 65 sr at 532 nm), clean continent (LR = 35 sr at 532 nm) and marine (LR = 20 sr at 532 nm). The uncertainties on aerosol extinction coefficients are within ± 40% assuming an uncertainty of 30% on LR (Omar *et al.*, 2009). Plus, CALIOP's low signal-to-noise ratio in daytime which could lead to the misclassification and/or lack of aerosol layer identification, and the calibration coefficient biases in the CALIOP daytime attenuated backscatter coefficient profiles would also contribute to the uncertainties (Kacenelenbogen *et al.*, 2011). Details of the retrieval algorithm can be found in the CALIOP Lidar Level-2 Algorithm Theoretical Basis Document (ATBD).

The daytime vertical aerosol extinction profiles and column AODs derived from CALIOP used in this study were obtained from the CALIOP Level-2 5 km Aerosol Profile version 3.01 data products. The data were chosen on a 2° × 2° scale (30°–32°N, 120°–122°E), and several factors such as cloud and uncertainties were taken into consideration to guarantee the accuracy of data.

METHODOLOGY

Determination of Angstrom Parameter

The Angstrom parameters were obtained from daily mean AODs (500 nm–675 nm) using the Angstrom formula:

$$\tau_{a\lambda} = \beta\lambda^{-\alpha} \tag{1}$$

where $\tau_{a\lambda}$ is the aerosol optical depth at wavelength λ, β is Angstrom's turbidity coefficient which indicates atmospheric turbidity, and α is Angstrom exponent that depends on the size distribution parameter of aerosols (Angstrom, 1961). This formula is based on the assumption that the aerosol extinction of solar radiation is a continuous function of wavelength without selective bands or lines for scattering or absorption (Rana *et al.*, 2009).

Comparison of CALIOP AODs with Ground-based Observations

To compare with the CALIOP AODs at 532 nm, AODs at 500 nm from sun photometer were converted to AODs at 532 nm using the Eq. (1). The column AODs derived from CALIOP were screened depending on several factors such as uncertainties and cloud, then chosen and averaged on a 2° × 2° scale (30°–32°N, 120°–122°E). The standard deviation of spatial averaged CALIOP AODs were calculated and analyzed. As CALIPSO passes through Shanghai at about 5:00 UTC, only the field measurements around this time were chosen for comparison.

Air Mass Back Trajectory

In this study, the Hybird Single-Particle Lagrangian Integrted Trajectory 4 (HYSPLIT 4) model developed by NOAA Air Resources Laboratory (Draxler and Rolph, 2003), was applied to calculate air mass backward trajectories. And the meteorological data used to initialize HYSPLIT was from the NCEP Global Date Assimilation System (GDAS) data set.

RESULTS AND DISCUSSION

AOD and Angstrom Exponent

Table 1 illustrates monthly averaged AODs (500 nm) and Angstrom exponent (500 nm–675 nm), and their tendencies are showed in Fig. 1. Most monthly-averaged AODs were

within the range of 0.20–0.60. The maximum AOD occured in November with value of 0.69, and the minimum appeared in August about 0.24. For Angstrom exponent (α), the range of variety was mainly from 1.20 to 1.50 except March, April and May. The maximum α appeared in September with 1.48 and the minimum appeared in March with 0.87.

Some previous studies suggest that the maximum AOD over Shanghai always occurs in summertime due to the raise of water vapor and aerosol hygroscopic growth (Li *et al.*, 2007; Pan *et al.*, 2010). However, considerable low AODs appeared during summertime in this experiment period, probably because of the effects of measures in transportation, energy and construction industries, and other relative aspects taken by the Shanghai municipal government to improve the city's air quality before and during the EXPO. The improvement in the ambient concentration of PM_{10}, SO_2, and NO_2 for recent years registered the relative success of these efforts (UNEP Environmental Assessment, EXPO 2010, Shanghai, China, 2009). Hara *et al.* (2011) observed a 'summer trough' pattern of the spherical AOD in Guangzhou and Hedo due to the seasonal air mass exchange. Ge *et al.* (2011) reported a lower acidity of summer precipitation in Central China caused by strong East Asian summer monsoon. In light of these result, the summer monsoon which comes from the ocean and brings clean maritime air mass to improve the diffusion of pollutants is correlated to the low AODs of Shanghai in summertime. In addition, the remarkable increase of precipitation in summer due to monsoon could also decrease the concentration of atmospheric aerosols (Bhaskar *et al.*, 2010).

A remarkable seasonal variation of α can be seen in Fig. 1. Low values of α only occured in spring, while in other seasons it was mostly above 1.30. It illustrates dominance of accumulation mode aerosols in summer, autumn and winter, and the particulate pollutants are mainly from anthropogenic emissions. Dominance of coarse mode aerosols indicated by low values of α in springtime is probably resulted from the long-distance transport of dust particles from Mongolia and northwest China (Gong *et al.*, 2003; Bian *et al.*, 2011).

The chemical reactions of SO_2 and NO_x play a considerable role in the atmospheric pollution of urban area (Seinfeld and Pandis, 2006; Wang *et al.*, 2006; Katzman *et al.*, 2010). And a certain correlation between AOD and particle concentration

Table 1. Monthly mean AOD and Angstrom exponent at Shanghai.

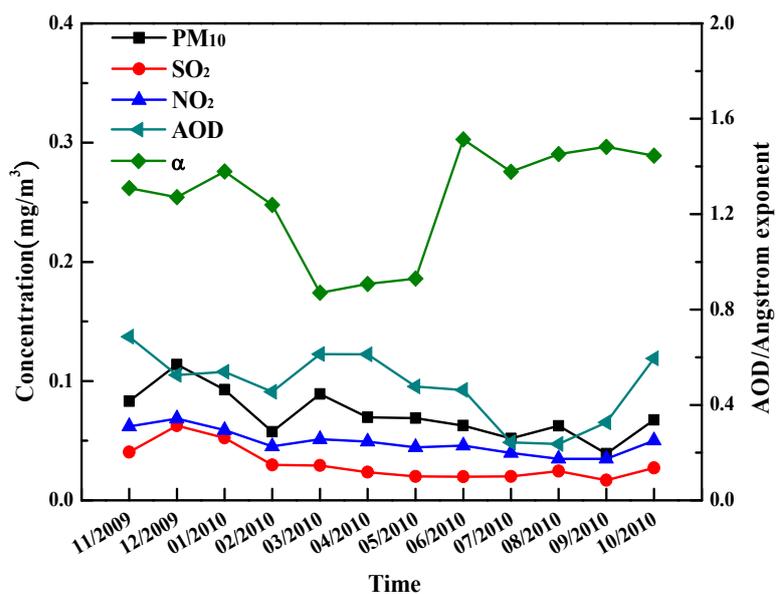| Date	AOD (500 nm)	A (500 nm–675 nm)	Rainfall (mm)	Day
Nov.	0.69 ± 0.15	1.31 ± 0.31	65.0	12
Dec.	0.53 ± 0.23	1.27 ± 0.21	31.3	11
Jan.	0.54 ± 0.11	1.38 ± 0.10	43.9	8
Feb.	0.45 ± 0.07	1.24 ± 0.20	70.8	6
Mar.	0.61 ± 0.31	0.87 ± 0.19	194.5	11
Apr.	0.61 ± 0.22	0.91 ± 0.28	80.6	10
May	0.48 ± 0.19	0.93 ± 0.21	75.1	6
Jun.	0.46 ± 0.23	1.51 ± 0.24	95.8	6
Jul.	0.24 ± 0.25	1.38 ± 0.19	183.3	6
Aug.	0.24 ± 0.14	1.45 ± 0.36	262.7	12
Sep.	0.33 ± 0.22	1.48 ± 0.27	246.4	15
Oct.	0.60 ± 0.17	1.44 ± 0.27	75.3	13

Fig. 1. Variation of monthly aerosol optical depth (AOD), Angstrom exponent (α) and concentrations of PM_{10}, SO_2 and NO_2 from Nov. 2009 to Oct. 2010.

is indicated by several studies (Engel-Cox *et al.*, 2005; Donkelaar *et al.*, 2006). The relationships between concentrations of PM_{10}, SO_2, and NO_2 converted from Air Pollution Index which has been monitored by Shanghai Environmental Protection Bureau (www.envir.gov.cn) and AODs are discussed in this study. As seen in Fig. 1, the concentrations of PM_{10}, SO_2 and NO_2 were mainly low from February to September 2010 except for March when dust storms happened frequently in the northwest of China, and then dust particles might transport to Shanghai and significantly contribute to the increase of PM_{10}. For other seasons, SO_2, NO_2 and PM_{10} emissions in Shanghai were mainly from industries, coal-fired power plants, transportation, construction and other local sources. Peaks of PM_{10}, NO_2 and SO_2 concentrations appeared in wintertime, indicating that the high AODs from November 2009 to January 2010 may primarily be contributed by local pollution and chemical reactions of NO_2 and SO_2. The variation of AODs shows a general consistency with PM_{10} concentrations especially from February to July 2010, and their correlation coefficient is about 0.41.

As one of the most widely used indices of atmospheric turbidity, Angstrom's turbidity coefficient (β) represents the combined effects of both scattering and absorption of aerosols. Angstrom exponent (α) is related to the size distribution of aerosols. Correlation between β and α in the spectral ranges of 500 nm–675 nm of different seasons is given in Fig. 2, The poor correlation of these two indices indicated that atmospheric turbidities were dominated by multiple sources of pollutant in different seasons. As the most developed city in China, aerosol emissions in Shanghai include both local pollution (mainly are anthropogenic sources), and long-distance transport of aerosols from inland and ocean (sea salt, dust, etc.) (Wang *et al.*, 2006). There is remarkable seasonal variation of β and α. As showed in Fig. 2, the most turbid situation occurred in spring. Since

the low values of α illustrated the dominance of coarse mode aerosols, the turbidity might be mainly caused by dust particles. Most of clear days appeared in summer when there were both low and high values of α, indicating the existence of both coarse (probably maritime aerosols) and fine particles.

Fig. 3 illustrates the frequency distributions of AODs and α during the period of observation. The bin intervals for AODs at 500 nm and α between 500 and 675 nm were set up to 0.20. Frequency of AODs shows an obvious single peak (0.30–0.40) distribution, and the range of values is primarily from 0.10 to 0.70, accounting for 91.4% of total occurrence. For α, the frequency histogram shows two peaks, indicating effects of both coarse and fine particles. The range of α varies mainly from 0.80 to 1.70 accounting for 89.2% with two peaks between 0.70–0.80 and 1.20–1.30, respectively.

Vertical Distribution of Aerosols

The aerosol extinction (σ) profiles derived from CALIOP were classified into three types in order to better describe the complex vertical characteristics of aerosols. Rules for classifying the three types are listed in Table 2, and the σ profiles are showed in Fig. 4. Three factors including temperature, relatively humidity (RH) and wind shears (the vertical gradient of wind speeds) were chosen for identifying the σ vertical characteristics. The corresponding temperature and RH profiles are derived from the GEOS-5 data product provided to the CALIPSO project by GMAO Data Assimilation System (Rienecker *et al.*, 2008), and the wind shears are derived from GDAS1 windgram developed by NOAA Air Resources Laboratory (http://ready.arl.noaa.gov/READYamet.php).

Figs. 4(a) and 4(d) shows the σ profiles of type I (20 September 2010). Aerosols were mainly concentrated near surface due to a weak inversion layer around 1.2 km which may confine aerosols in mixing layer. Above the inversion
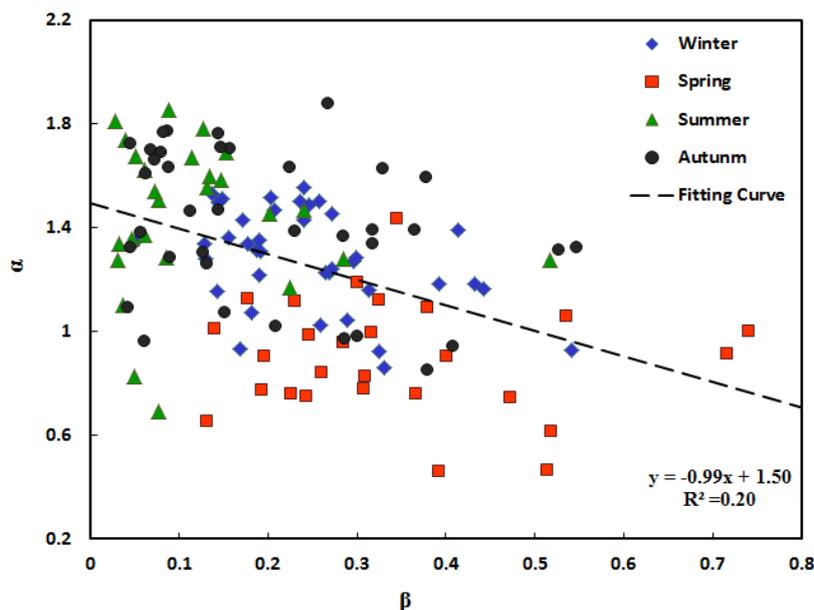
Fig. 2. Scatterplots of Angstrom exponent (α) versus Angstrom's turbidity coefficient (β) for different seasons.
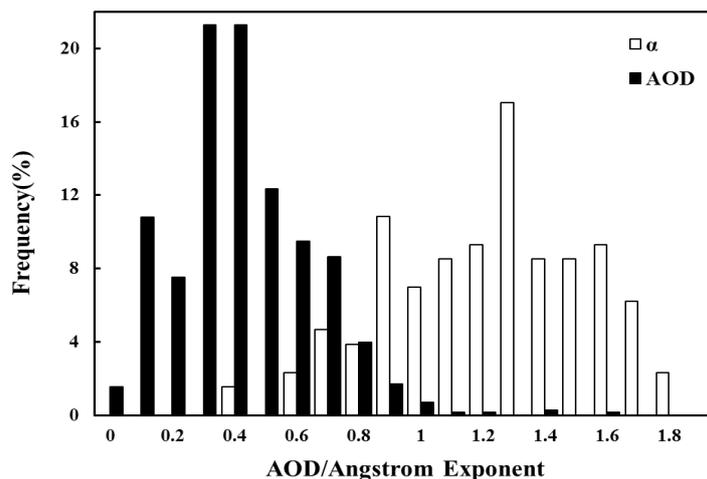

Fig. 3. Frequency distribution of daily AOD and Angstrom exponent.

layer, σ dramatically decreased with the increase of altitude. Wind profile from top to the base of the aerosol layer showed that the wind speed was generally high, especially above 1.5 km which may improve the diffusion of pollutants. Source of aerosols of this type is probably local pollution, and the particles above inversion layer could be local aerosols lifted up by wind and aerosols remained in residual layer.

For type II case (4 November 2009), CALIOP captured a well-mixed layer, in which aerosol-rich air mass was mixed up to nearly 1.8 km with a maximum extinction near the aerosol layer top. The relatively strong inversion layer around 1.3 km showed in Fig. 4(e) would confine aerosols to the region below inversion layer, and wind speed kept low within the whole aerosol layer. Good correlations between high values of σ and RH around 1.5 km implied that aerosol scattering coefficients might be enhanced because of hygroscopic growth effect, normally for RH greater than 70% (Hanel, 1976; Fitzgerald *et al.*, 1982; He

et al., 2008). This type of aerosol vertical distribution may mainly be attributed to the presence of convectively driven surface-emitted aerosols which tend to accumulate below inversion layer. Moreover, the aerosols remained in residual layer and aerosols from long-range transport may also play a part. However, it is hard to separate the contribution of aerosols from different sources in type II condition.

Type III which showed in Figs. 4(c) and 4(f) is more complicated than the above two types. To better describe the vertical characteristics of this type, two sub-categories were classified depend on whether inversion happened (III-i) or not (III-ii). For the case of 8 February 2010, showed in black line in Figs. 4(c) and 4(f), more than one aerosol layer were captured besides near-surface one. Since the inversion layer around 0.5 km would confine local aerosols to the region below 0.5 km, it was clear that the source of near-surface layer was local pollutants And the upper aerosol layers which separated obviously from the near surface one

Table 2. Classification of aerosol extinction vertical profile of 15 cases.*

Type	Classification Rules	Cases
I	1. The columnar τ_{532nm} is greater than 0.1 2. Only one remarkable and isolated aerosol layer shows near surface 3. σ increases as the altitude decreases, and the peak value appears near surface	22 Dec. 2009 9 Sep. 2010
II	1. Same as rules 1-2 in Type I 2. σ shows no remarkable change as the altitude decreases within the near surface aerosol layer	4 Nov. 2009 6 Dec. 2009 4 Sep. 2010 6 Oct. 2010
III(i/ii)	1. Same as rules 1-2 in Type I 2. There are other aerosol layers above the near surface one 3. The joint between different layers shows relative low σ 4. Can be classified into two conditions depend on whether inversion layer appears(i) or not(ii)	7 Jan. 2010 8 Feb. 2010 22 Oct. 2010 28 Mar. 2010 29 Apr. 2010 31 May 2010 16 Jun. 2010 18 Jul. 2010 19 Aug. 2010

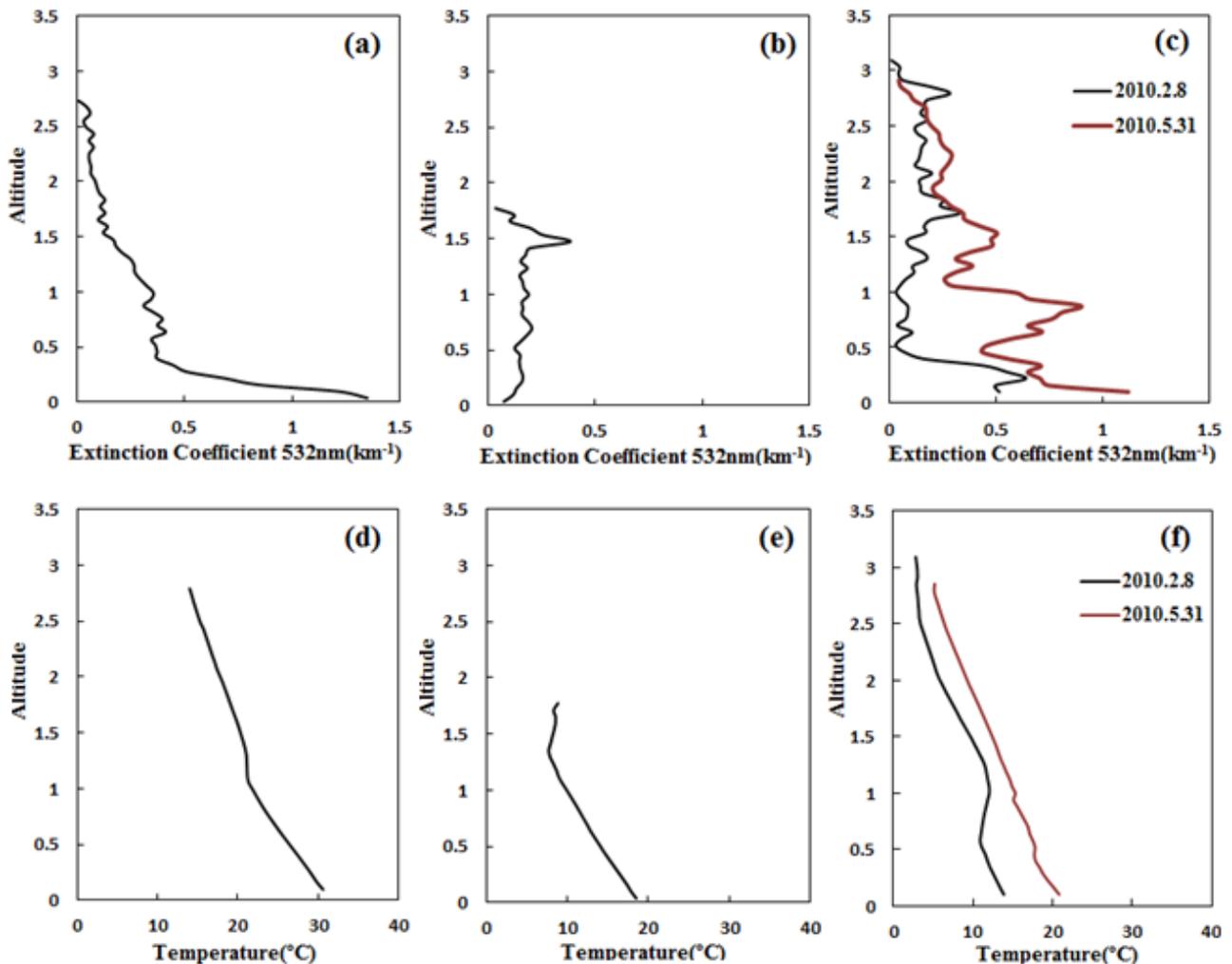* Some rules are with reference to Wang *et al.* (2010).

Fig. 4. Mean vertical profiles of aerosol extinction coefficient at 532 nm derived from CALIOP for (a) type I (at 4:44 UTC on 20 Sep. 2010), (b) type II (at 4:49 UTC on 4 Nov. 2009) and (c) type III-i (at 4:44 UTC on 8 Feb. 2010) and type III-ii (at 4:54 UTC on 31 May 2010). Plots of (d), (e), (f) are same as (a), (b), (c) but for temperature from GEOS-5 products provided to the CALIPSO project by the GMAO Data Assimilation System.

was probably resulted in long-range transport of aerosols. The wind speed kept low near surface and became much higher within upper layers. Compare to type III-i, there was no apparent inversion for type III-ii. Thus, although more than one remarkable aerosol layers were captured by CALIOP, it was hard to identify the source of each layer. Three types of aerosols may be responsible: (1) local aerosols which may concentrate near surface or be lifted up to the upper layer; (2) aerosols remained in the residual layer; (3) aerosols transported from remote sources.

The classification of all the 15 cases is showed in Table 2. Type I, II and III were found in 2, 4 and 9 cases (3 for III-i, 6 for III-ii), respectively. For the 15 cases, type I and II conditions happened in autumn and winter, while type III mainly appeared in spring and summer when inversion barely happened. However, the classification of σ vertical profiles applied in this study is only an approximation. All the σ profiles given is only represent the situation around 5:00 UTC, and the spatial average calculation of σ profiles may smooth the results and bring uncertainties besides those of CALIOP and its retrieval algorithm.

Back Trajectory Analysis

Backward trajectory analysis is an effective and simple way to diagnose the movement of air mass. 5-day backward trajectories of the 15 cases which discussed in the previous section are showed in Fig. 5. The heights of maximum extinction of near-surface layer and the top of upper layer for type III/the top of near-surface layer for type I and II were chosen to present the near-surface (Fig. 5(a)) and upper layer (Fig. 5(b)) air mass transport, respectively, and the trajectory altitudes are illustrated by color bars. This section would provide a brief discussion of backward trajectories in relation to σ vertical profiles classification (Table 2).

For type I condition (only one remarkable and isolated near-surface aerosol layer were observed, and σ decreased as altitude increased) the two cases had different air mass pathways. For the case of 22 December 2009, the trajectory denoted that air masses came from northwest or west of China, passed over several provinces of the YRD, and then reached Shanghai. Thus it may bring some anthropogenic emissions to Shanghai. For another case of type I (20 September 2010), affected by summer monsoon, the air mass traversed over the East China Sea and probably brought some clear air and marine aerosols. Therefore, local pollutant would be main source of aerosols for this case. In general, the anthropogenic aerosols due to local pollution and long-range transport play a main role in cases of Type I condition.

The 5-day backward trajectories of type II cases show similar patterns. Except two eastern trajectories (4 September 2010) probably affected by summer monsoon, the rest trajectories mainly originated from northwest or north of China, and passed over the yellow sea/east sea of China. Previous study denotes that more aerosol water uptake or hydroscopic growth would happen when near surface shallow transport with anthropogenic aerosols over the ocean (Seinfeld, 1986; Kolev *et al.*, 2000). Since most trajectories for near surface layer were within 1 km when traversed over sea, the long-range transport pollution may be one of the sources of aerosols besides local ones. As same as type I, anthropogenic aerosols could be the main contributor to aerosol loading for the 4 cases of type II over Shanghai.

In contrast to type I and II, Type III shows more complicated characteristics. For type III-i cases, the 5-day backward trajectories of upper layer were mainly from the west of China and traveled over the YRD except 22 October case, while the near surface trajectories were different from each other. Besides long-range transport of aerosols, inversion which prevents mixing of vertical convective aerosols also plays an important role in the formation of multilayer aerosol structure of type III-i. For this sub-type condition, anthropogenic pollution still plays a significant part. However, for type III-ii, long-distance transport of aerosols would be the main factor of the multilayer structure formation. And three kinds of aerosols may contribute to the upper layer: (1) dust from Mongolia and northwest part of China which denoted by westerly trajectories in spring; (2) sea salt from the marine region which illustrated by easterly trajectories in summer; (3) smoke due to biomass burning which are from surrounding areas of Shanghai such as Anhui province (Li *et al.*, 2010).

An obvious seasonal characteristic can be summarized from the trajectories. The air masses were mainly from inland in spring, autumn and winter, while in summertime, monsoon from the sea would bring clean air to Shanghai. And the trajectories also denote some near-surface transport of aerosols from surrounding areas of Shanghai. It means that measures should not be only taken in Shanghai but also in its neighboring provinces to improve the air quality.

Comparison of AODs Derived from CALIOP and Sun Photometer

Determination of lidar ratio (LR) which based on the aerosol type, aerosol layer elevation and optical, geographical and temporal characteristics of aerosols plays an important role in the retrieval of aerosol extinction profiles and optical depth. However, as the number of MPLNET sites is very limited, particularly in areas outside the United State at present time, and the understanding about vertical distribution of aerosols is not full-established yet, there is still large uncertainties in the CALIOP retrieval of aerosols especially when it faces a wide variety of aerosol types over land (Royer *et al.*, 2010; Kacenelenbogen *et al.*, 2011; Kittaka *et al.*, 2011).

Comparison of retrieved AODs derived from CALIOP with those from ground-based observation is showed in Fig. 6. The AODs derived from CALIOP and sun photometer agree generally with a linear relationship as $AOD_{observation} = AOD_{CALIPSO} \times 0.97 + 0.08$ ($R^2 = 0.59$). An underestimation of CALIOP-derived AODs can be noticed clearly. Of all the nine cases, three ones are beyond the error range of $\Delta\tau = \pm 0.05 + 0.2\tau$. And all the error bars on the dots overlay with error range, representing some information in regard to variation of CALIOP-derived AODs along the satellite track. Kittaka *et al.* (2011) have compared the AOD derived from CALIOP and MODIS-Aqua from June 2006 to August 2008 on global scale, showing that complex situation over
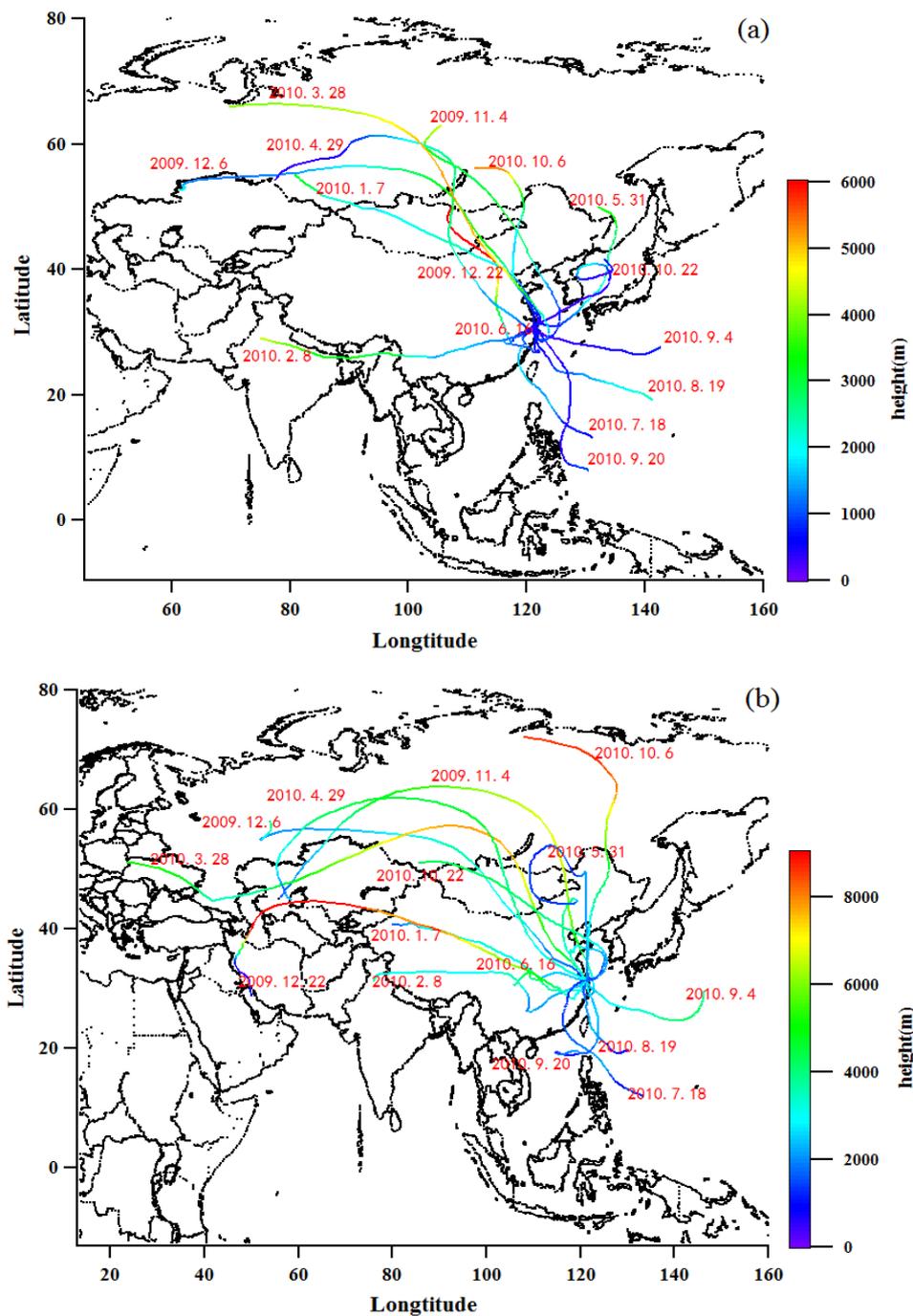
Fig. 5 Back trajectories arriving at site (31.17°N, 121.30°E) at 5:00 UTC above the heights of (a) maximum extinction within near-surface layer and (b) top of the upper layer.

land such as wide variety of aerosol types may introduce uncertainty in choosing aerosol model and LR used in retrieval of CALIOP-derived AODs. Besides, several other different factors that are often related to each other can also lead to uncertainty, such as detection of aerosol layer base height, CALIOP's low signal-to-noise ratio in daytime, and the calibration coefficient biases in the CALIOP daytime attenuated backscatter coefficient profiles etc. As the number of cases is limited in this study, more data are needed to better evaluate the accuracy of CALIOP-derived AODs over Shanghai.

CONCLUSION

Aerosol optical properties over Shanghai from November 2009 to October 2010 were analyzed using both ground and satellite measurements. Study of column AODs and α over Shanghai shows remarkable seasonal variation. The values of α were mainly above 1.30 except springtime, indicating the dominance of fine particles over Shanghai. Maximum and minimum AOD occurred in November with 0.69 and August with 0.24, respectively. AODs mainly accumulate between 0.10 and 0.70, while α varies basically from 0.80
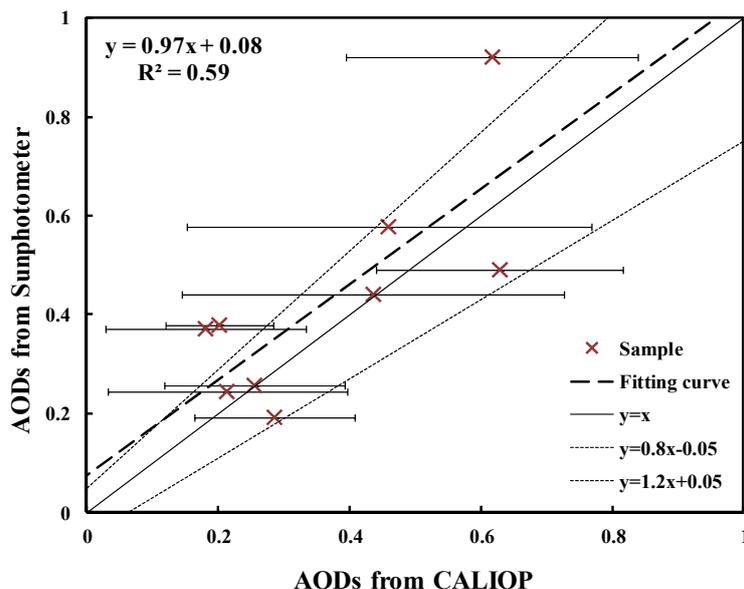
Fig. 6. Comparison between of AODs derived from CALIOP and Sun photometer on 4 Nov., 6 and 22 Dec. 2009, 7 Jan., 8 Feb., 19 Aug., 4 and 20 Sep., 6 Oct. 2010). The error bars on dots along x-axis denote the standard deviation of spatial mean CALIOP AODs.

to 1.70. Relationship of AODs and α with concentrations of PM_{10}, SO_2, and NO_2 are discussed. And the correlation between PM_{10} and AOD is 0.41.

The aerosol extinction (σ) profiles derived from CALIOP were classified into three types and discussed in consideration of temperature, relatively humidity and wind shears. All the three factors have different effect on σ profiles, and temperature is the most obviously one especially when inversion happens. Local pollution is the main source of type I and II profiles, while type III profiles represent the effect of both long-range transport of aerosols and local emissions. 5-day backward trajectories denote three possible sources of aerosols over shanghai besides local emission: (1) dust from Mongolia and northwest part of China; (2) sea salt from the sea; (3) smoke due to biomass burning from some surrounding areas of Shanghai. Both backward trajectories and the analysis of correlation between atmospheric turbidity and Angstrom exponent prove the multiple sources of pollution over Shanghai which would complicate the aerosol optical properties of the city.

Comparison of retrieved AODs derived from CALIOP and sun photometer shows a general agreement with $AOD_{observation} = AOD_{CALIPSO} \times 0.97 + 0.08$ ($R^2 = 0.59$), and CALIOP data appears to underestimate the values of AOD. The different spatial range between the AODs derived from CALIOP with ground measurements, the assumption of lidar ratio and other factors such as relative low signal-to-noise ratio of CALIOP daytime data would contribute to the uncertainties of CALIOP derived AODs.

ACKNOWLEDGEMENTS

REFERENCES

Angstrom, A. (1964). The Parameters of Atmospheric Turbidity. *Tellus* 16: 64–75.

Bhaskar, B.V. and Mehta, V.M. (2010). Atmospheric Particulate Pollutants and their Relationship with Meteorology in Ahmedabad. *Aerosol Air Qual. Res.* 10: 301–315

Bian, H, Tie, X.X., Cao, J.J., Ying, Z.M., Han, S.Q. and Xue, Y. (2011). Analysis of a Severe Dust Storm Event over China: Application of the WRF-Dust Model. *Aerosol Air Qual. Res.* 11: 873–882

Chen, Y.H., Mao, X.Q., Huang, J.P., Zhang, H., Tang, Q., Pan, H. and Wang, C.H. (2009). Vertical Distribution Characteristics of Aerosol during a Long-distance Transport of Heavy Dust Pollution. *China Environ. Sci.* 29: 449–454.

Chiang, C.W., Chen, W.N., Liang, W.A., Das, S.K. and Nee, J.B. (2007). Optical Properties of Tropospheric Aerosols Based on Measurements of Lidar, Sun Photometer, and Visibility at Chung-Li (25°N, 121°E). *Atmos. Environ.* 41: 4128–4137.

Donkelaar, A.V., Martin, R.V. and Park, R.J. (2006). Estimating Ground-level PM$_{2.5}$ Using Aerosol Optical Depth Determined from Satellite Remote Sensing. *J.*

Geophys. Res. 111: D21201, doi: 10.1029/2005JD006996.

Draxler, R.R. and Rolph, G.D. (2003). HYSPLIT (HYbrid Single-Particle Lagrangian Integrated Trajectory) Model Access Via NOAA ARL READY. NOAA Air Resources Laboratory, Silver Spring, MD. Website: http://www.arl.noaa.gov/ready/hysplit4.html.

Duan, J. and Mao, J. (2007). Study on the Distribution and Variation Trends of Atmospheric Aerosol Optical Depth over the Yangtze River Delta. *Acta Scien. Circum.* 27: 537–543.

Engel-Cox, J.A., Young, G.S. and Hoff, R.M. (2005). Application of Satellite Remote-sensing Data for Source Analysis of Fine Particulate Matter Transport Events. *J. Air Waste Manage. Assoc.* 55: 1389–1397.

Fitzgerald, J.W., Hoppel, W.A. and Vietti, M.A. (1982). The Size and Scattering Coefficient of Urban Aerosol Particles at Washington, DC as a Function of Relative Humidity. *J. Atmos. Sci.* 39: 1838–852.

Ge, B.Z., Wang, Z.F., Xu, X.B., Tang, J., He, Y.J., Uno, I. and Ohara, T. (2011). Impact of the East Asian Summer Monsoon on Long-term Variations in the Acidity of Summer Precipitation in Central China. *Atmos. Chem. Phys.* 11: 1671−1684.

Gong, S.L., Zhang, X.Y., Zhao, T.L., McKendry, I.G., Jaffe, D.A. and Lu, N.M. (2003). Characterization of Soil Dust Aerosol in China and its Transport and Distribution during 2001 ACE-Asia: 2 Model Simulation and Validation *J. Geophys. Res.* 108: 4262, doi: 10.1029/2002JD002633.

Hanel, G. (1976). The Properties of Atmospheric Aerosol Particles as Function of the Relative Humidity at Thermodynamic Equilibrium with the Surrounding Atmosphere. *Adv. Geophys.* 19: 73−188.

Hara, Y., Uno, I., Shimizu, A., Sugimoto, N., Matsui, I., Yumimoto, K., Kurokawa, J.I., Ohara, T. and Liu, Z.Y. (2011). Seasonal Characteristics of Spherical Aerosol Distribution in Eastern Asia: Integrated Analysis Using Ground/Space-Based Lidars and a Chemical Transport Model. *SOLA* 7: 121−124.

Hatakeyama, S., Hanaoka, S., Ikeda, K., Watanabe, I., Arakaki, T., Sadanaga, Y., Bandow, H., Kato S., Kajii, Y., Sato, K., Shimizu, A. and Takami, A. (2011). Aerial Observation of Aerosols Transported from East Asia — Chemical Composition of Aerosols and Layered Structure of an Air Mass over the East China Sea. A*erosol Air Qual. Res.* 11: 497–507

He, Q., Li, C., Mao, J., Lau, A. K.H. and Chu, D.A. (2008). Analysis of Aerosol Vertical Distribution and Variability in Hong Kong. *J. Geophys. Res.* 113: D14211, doi: 10.1029/2008JD009778.

He, Q.S., Li, C.C., Tang, X., Li, H.L., Geng, F.H. and Wu, Y.L. (2010). Validation of MODIS Derived Aerosol Optical Depth over the Yangtze River Delta in China. *Remote Sens. Environ.* 114: 1649–1661.

Huang, J.P., Huang, Z.W., Bi, J.R., Zhang, W. and Zhang, L. (2008b). Micro-Pulse Lidar Measurements of Aerosol Vertical Structure over the Loess Plateau. *Atmos. Oceanic Sci. Lett.* 1: 8–11.

Huang, J.P., Minnis, P., Chen, B., Huang, Z.W., Liu, Z.Y., Zhao, Q.Y., Yi, Y.H. and Ayers, J.K. (2008a). Long-range Transport and Vertical Structure of Asian Dust from CALIPSO and Surface Measurements during PACDEX. *J. Geophys. Res.* 113: D23212, doi: 10.1029/2008JD010620.

Hunt, W.H., Winker, D.M., Vaughan, M.A., Powell, K.A., Lucker, P.L. and Weimer, C. (2009). CALIPSO Lidar Description and Performance Assessment. *J. Atmos. Oceanic Technol.* 26: 1214–1228.

Ichoku, C., Robert, L., Kaufman, Y.J., Remer, L.A., Li, R.R., Martins, V.J., Holben, B.N., Abuhassan, N., Slutsker, I., Eck, T.F. and Christophe, P. (2002). Analysis of the Performance Characteristics of the five-channel Microtops II Sun Photometer for Measuring Aerosol Optical Thickness and Perceptible Water Vapor. *J. Geophys. Res.* 107: 4179, doi: 10.1029/2001JD001302.

Intergovernmental Panel on Climate Change (2007). *Climate Change 2007, Working Group I Report—The Physical Science Basis*, Solomon, S. *et al.*, (Eds.), Cambridge Univ. Press, New York.

Kacenelenbogen, M., Vaughan, M.A. Redemann, J., Hoff, R.M., Rogers, R.R., Ferrate, R.A., Russell, P.B., Hostetler, C.A., Hair, J.W. and Holben, B.N. (2011). An Accuracy Assessment of the CALIOP/CALIPSO Version 2/Version 3 Daytime Aerosol Extinction Product Based on a Detailed Multi-Sensor, Multi-Platform Case Study. *Atmos. Chem. Phys.* 11: 3981–4000.

Katzman, T.L., Rutter, A.P., Schauer, J.J., Glynis C. Lough, G.C., Kolb, C.K. and Klooster, S.V. (2010). $PM_{2.5}$ and $PM_{10–2.5}$ Compositions during Wintertime Episodes of Elevated PM Concentrations across the Midwestern USA. A*erosol Air Qual. Res.* 10: 140–153

Kaufman, Y.J., Tanre, D., Gordon, H.R., Nakajima, T., Lenoble, J., Frouin, R., Grassl, H., Hermann, B.M., King, M.D., and Teillet, P.M. (1997). Passive Remote Sensing of Tropospheric Aerosol and Atmospheric Correction for the Aerosol Effect. *J. Geophys. Res.* 102: 16815–16830, doi: 10.1029/97JD01496.

Kittaka, C., Winker, D.M., Vaughan, M.A., Omar, A. and Remer, L.A. (2011). Inercomparison of Column Aerosol Optical Depths from CALIPSO and MODIS-Aqua. *Atmos. Meas. Tech.* 4: 131–141.

Kolev, I., Skakalova, T. and Grogorov, I. (2000). Lidar Measurement of Aerosol Extinction Profile in a Coastal Zone of the Bulgarian Black Sea. *Atmos. Environ.* 34: 3813–3822.

Li, H.Y., Han, Z.W., Cheng, T.T., Du, H.H., Kong, L.D., Chen, J.M., Zhang, R.J. and Wang, W.J. (2010). Agricultural Fire Impacts on the Air Quality of Shanghai during Summer Harvest time. *Aerosol Air Qual. Res.* 10: 95–101.

Li, Z., Xia, X., Cribb, M., Mi, W., Holben, B., Wang, P., Chen, H., Tsay, S.C., Eck, T.F., Zhao, F., Dutton, E.G. and Dickerson, R.R (2007). Aerosol Optical Properties and their Radiative Effects in Northern China. *J. Geophys. Res.* 112: D22S01, doi: 10.1029/2006JD007382.

Luo, Y., Lu, D., Zhou, X. and Li, W. (2002). Analyses on the Spatial Distribution of Aerosol Optical Depth over China in Recent 30 Years. *Chin. J. Atmos. Sci.* 26: 721–730.

Morys, M., Mims, F.M., Hagerup, S., Anderson, S.E., Baker,

A., Kia, J. and Walkup, T. (2001). Design, Calibration and Performance of MICROTOPS II Hand-held Ozone Monitor and Sun Photometer. *J. Geophys. Res.* 106: 14573–14582, doi: 10.1029/2001JD900103.

Murayama, T., Müller, D., Wada, K., Shimizu, A., Sekiguchi, M. and Tsukamoto, T. (2004). Characterization of Asian Dust and Siberian Smoke with Multi-wavelength Raman Lidar over Tokyo, Japan, in spring 2003. *Geophys. Res. Lett.* 31: L23103 doi: 10.1029/2004GL021105.

Nakajima, T., Yoon, S.C., Ramanathan, V., Shi, G.Y., Takemura, T., Higurashi, A., Takamura, T., Aoki, K., Sohn, B.J., Kim, S.W., Tsuruta, H., Sugimoto, N., Shimizu, A., Tanimoto, H., Sawa, Y., Lin, N.H., Lee, C.T., Goto, D. and Schutgens, N. (2007). Overview of the Atmospheric Brown Cloud East Asian Regional Experiment 2005 and a Study of the Aerosol Direct Radiative Forcing in East Asia. *J. Geophys. Res.* 112: D24S91, doi: 10.1029/2007JD009009.

Pan, L., Che, H.Z., Geng, F.H., Xia, X.G., Wang, Y.Q., Zhu, C.Z., Chen, M., Gao, W. and Guo, J.P. (2010). Aerosol Optical Properties Based on Ground Measurements over the Chinese Yangtze Delta Region. *Atmos. Environ.* 44: 2587–2596.

Ping, L.S. (2009). *UNEP Environmental Assessment, EXPO 2010, Shanghai, China*, Produced by the UNEP Division of Communications and Public Information, China.

Rana, S., Kant, Y. and Dadhwal, V. K. (2009). Diurnal and Seasonal Variation of Spectral Properties of Aerosols over Dehradun, India. *Aerosol Air Qual. Res.* 9: 32–49.

Rienecker, M.M., Suarez, M.J., Todling, R., Bacmeister, J., Takacs, L., Liu, H.C., Gu, W., Sienkiewicz, M., Koster, R.D., Gelaro, R., Stajner, I. and Nielsen, J.E. (2008). The GEOS-5 Data Assimilation System - Documentation of Versions 5.0.1, 5.1.0, and 5.2.0, In *Technical Report Series on Global Modeling and Data Assimilation*, Vol. 27.

Royer, P., Raut, J.C., Ajello, G., Berthier, S. and Chazette, P. (2010). Synergy between CALIOP and MODIS Instruments for Aerosol Monitoring: Application to the Po Valley. *Atmos. Meas. Tech.* 3: 893–907.

Seinfeld, J.H. (1986). *Atmospheric Chemistry and Physics of Air Pollution*, John Wiley & Sons, New York, USA.

Seinfeld, J.H. and Pandis, S.N. (2006). *Atmospheric Chemistry and Physics: From Air Pollution to Climate Change (2nd ed.)*, John Wiley & Sons, New York, USA. p. 57–58 and p. 381–383.

Shimizu, A., Sugimoto, N., Matsui, I., Arao, K., Uno, I., Murayama, T., Kagawa, N., Aoki, K., Uchiyama, A. and Yamazaki, A. (2004). Continuous Observations of Asian Dust and Other Aerosols by Polarization Lidar in China and Japan during ACE-Asia. *J. Geophys. Res.* 109: D19S17, doi: 10.1029/2002JD003253.

Wang, S.H., Lin, N.H., Chou, M.D., Tsay, S.C., Welton, E.J., Hsu, N.C., Giles, D.M., Liu, G.R. and Holben, B.N. (2010). Profiling Transboundary Aerosols over Taiwan and Assessing their Radiative Effects. *J. Geophys. Res.* 115: D00K31, doi: 10.1029/2009JD013798.

Wang, Y., Zhuang, G.S., Zhang, X.Y., Huang, K., Xu, C., Tang, A.H., Chen, J.M. and An, Z.S. (2006). The Ion Chemistry, Seasonal Cycle, and Sources of $PM_{2.5}$ and TSP Aerosol in Shanghai. *Atmos. Environ.* 40: 2935–2952.

Welton, E.J., Campbell, J.R., Spinhirne, J.D. and Scott, V.S. (2001). Global Monitoring of Clouds and Aerosols Using a Network of Micropulse Lidar Systems. *Proc. SPIE Int. Soc. Opt. Eng.* 4153: 151–158.

Winker, D.M., Pelon, J., Coakley Jr., J.A., Ackerman, S.A., Charlson, R.J., Colarco, P.R., Flamant, P., Fu, Q., Hoff, R., Kittaka, C., Kubar, T.L., LeTreut, H., McCormick, M.P., Megie, G., Poole, L., Powell, K., Trepte, C., Vaughan, M.A. and Wielicki, B.A. (2010). The CALIPSO Mission: A Global 3D View of Aerosols and Clouds. *Bull. Am. Meteorol. Soc.* 91: 1211–1229.

Winker, D.M., Vaughan, M.A., Omar, A., Hu, Y., Powell, K.A., Liu, Z., Hunt, W.H. and Young, S.A. (2009). Overview of the CALIPSO Mission and CALIOP Data Processing Algorithms. *J. Atmos. Oceanic Technol.* 26: 2310–2323.

Xiao, Z.M., Zhang, Y.F., Hong, S.M., Bi, X.H., Jiao, L., Feng, Y.C. and Wang, Y.H. (2011). Estimation of the Main Factors Influencing Haze, Based on a Long-term Monitoring Campaign in Hangzhou, China. *Aerosol Air Qual. Res.* 11: 873–882.

Yu, H., Kaufman, Y.J., Chin, M., Feingold, G., Remer, L.A., Anderson, T.L., Balkanski, Y., Bellouin, N., Boucher, O., Christopher, S., DeCola, P., Kahn, R., Koch, D., Loeb, N., Reddy, M.S., Schulz, M., Takemura, T. and Zhou, M. (2006). A Review of Measurement-based Assessments of the Aerosol Direct Radiative Effect and Forcing. *Atmos. Chem. Phys.* 6: 613–666.

Yu, H.B., Chin, M., Winker, D.M., Omar, A.H., Liu, C.K. and Diehl, T. (2010). Global View of Aerosol Vertical Distributions from CALIPSO Lidar Measurements and GOCART Simulations: Regional and Seasonal Variations. *J. Geophys. Res.* 115: D00H30, doi: 10.1029/2009JD013364.

Zhang, R., Han, Z., Cheng, T. and Tao, J. (2009), Chemical Properties and Origin of Dust Aerosols in Beijing during Springtime. *Particuology* 7: 61–67.